Available online at www.sciencedirect.com
ScienceDirect
Journal of the European Ceramic Society 27 (2007) 4603–4611
www.elsevier.com/locate/jeurceramsoc

Creep damage resistance of ceramic–matrix composites

B. Wilshire *, M.R. Bache

Materials Research Centre, School of Engineering, University of Wales Swansea, Singleton Park, Swansea SA2 8PP, UK

Received 22 November 2006; received in revised form 20 March 2007; accepted 25 March 2007
Available online 12 June 2007

Abstract

The tensile creep and creep fracture properties in air at 1300 °C are documented for two ceramic fibre-reinforced ceramic–matrix composites (CFCMCs). These recently developed materials were produced with woven bundles of Hi-Nicalon™ fibres reinforcing either $A1_2O_3$ or enhanced SiBC matrices, allowing data comparisons to be made with similar CFCMCs having different fibre–matrix combinations. The results confirm that the longitudinal fibres govern the rates of strain accumulation and crack growth, but the fracture characteristics are determined by fibre failure caused by oxygen penetration as matrix cracks develop. The analysis then suggests that carbon fibre-reinforced doloma–matrix composites could offer a combination of creep-resistant fibres and creep damage-resistant matrices suitable for long-term load-bearing service in high-temperature oxidizing environments.

Keywords: Composites; Creep; Fracture; Damage resistance; Structural applications

1. Introduction

Since the 1950s, the introduction of new metallic materials and improved manufacturing technologies have supported major advances in the power, efficiency and reliability of aeroengines, underpinning impressive increases in the range, performance and safety of civil and military aircraft.[1,2] In seeking further gains in thrust-to-weight ratio and fuel economy, ceramic–matrix composites reinforced with continuous ceramic fibres (CFCMCs) represent a recognized material development opportunity. Even so, particularly as the civil aviation sector becomes increasingly cost conscious, emphasis must be directed towards product cost reduction as well as component life enhancement.

Although a wide variety of CFCMCs have been developed, special attention has been focussed on composites with either SiC or $A1_2O_3$ matrices, reinforced with interwoven bundles of silicon carbide fibres.[2,3] However, the creep fracture characteristics of these types of composite at high temperatures are adversely affected by oxidizing atmospheres,[4–6] i.e. the service conditions typically experienced by aeroengine components. For this reason, in the present study, creep property values determined in air at 1300 °C are documented for two advanced SiC fibre-reinforced products. These results are then discussed with reference to data sets reported for several related materials.[7–11] In this way, a straightforward evaluation can be made of the creep performance improvement achieved using

(a) different fibre types for composites with comparable matrices, fibre–matrix interfaces and fibre architectures and
(b) different matrices for composites having similar fibre types, fibre configurations and fibre–matrix interfaces.

By clarifying the principal creep life-limiting features of this product range, proposals are made for a relatively low-cost composite which may provide the creep damage resistance needed for high-temperature load-bearing applications involving prolonged exposure in oxidizing environments.

2. Experimental procedures

To quantify the effects of changing the reinforcing fibres, creep property measurements now recorded for two CFCMCs produced with high Hi-Nicalon™ fibres are compared with results available for similar composites containing Nicalon™ NLM202 fibres (Nippon Carbon Co., Japan). Hi-Nicalon™ fibres are characterized by superior elastic moduli and creep resistance, achieved through processing operations adopted to

* Corresponding author. Tel.: +44 1792 295243; fax: +44 1792 295244.
E-mail address: b.wilshire@swansea.ac.uk (B. Wilshire).

0955-2219/$ – see front matter © 2007 Elsevier Ltd. All rights reserved.
doi:10.1016/j.jeurceramsoc.2007.03.029

eliminate the amorphous silicon oxy-carbide phase (SiC_xO_y) which reduces the creep strength of Nicalon™ NLM202 fibres.[12,13]

To consider the effects of changing the matrix type, one of the present Hi-Nicalon™-reinforced composites had an alumina matrix, giving a material referred to as $HNSiC_f$–$A1_2O_3$. The other composite was prepared with an 'enhanced' SiC matrix, containing boron-based additives which form a sealant glass to limit oxygen penetration into the material during creep exposure.[14] This product is designated as $HNSiC_f$–SiBC.

For tensile creep tests carried out in air at 1300 °C, the behaviour patterns displayed by the $HNSiC_f$–$A1_2O_3$ and $HNSiC_f$–SiBC samples are analyzed in relation to data obtained under the same conditions for two groups of CFCMCs.

(a) The consequences of changing only the fibre type becomes apparent by comparing the creep properties of $HNSiC_f$–$A1_2O_3$ with those of an alumina–matrix composite reinforced with Nicalon™ NLM202 fibres, called SiC_f–$A1_2O_3$.[7] With both materials, the fibres were given a thin boron nitride coating before ~5 μm thick SiC coatings were deposited by chemical vapour infiltration (CVI), resulting in double BN/SiC interfaces. The $A1_2O_3$ matrices were then formed by in situ directional oxidation of liquid aluminium, as previously described for the SiC_f–Al_2O_3 specimens.[7]

(b) The $HNSiC_f$–SiBC samples relate to three different composites with SiC fibres reinforcing SiC matrices. All of these products were fabricated with carbon interfaces (~0.5 μm thick), before CVI processing to introduce the polycrystalline SiC matrices. However, the fibre–matrix combination differed, with
- Nicalon™ NLM202 fibres reinforcing[6,9] a standard SiC matrix (called SiC_f–SiC),
- Nicalon™ NLM202 fibres reinforcing[10] an 'enhanced' SiC matrix (called SiC_f–SiBC) and
- Hi-Nicalon™ fibres reinforcing[11] a standard SiC matrix (called $HNSiC_f$–SiC).

The principal distinguishing features of these CFCMCs are summarized in Table 1. Each composite contained approximately 40 vol.% fibres with average diameters of ~15 μm, incorporated as bundles of about 500 fibres woven to obtain 2D layers of fabric. The woven layers or plies were then aligned and stacked to produce preforms having balanced 0/90° architectures. Moreover, after the fibre coating and densification operations, all matrices had porosities of 15% or more. Specifically, small pores were present in the matrix regions within the fibre bundles, with large pores (termed macro-pores) between the plies and at yarn intersections within the plies.[7]

Having selected composites with similar 'macro-structures', comparable test procedures were used to determine the creep and creep fracture properties. Thus, for the present $HNSiC_f$–$A1_2O_3$ and $HNSiC_f$–SiBC materials, tensile creep tests were carried out in air at 1300 °C using a servo-hydraulic machine in load control mode. The load train included hydraulic wedge grips, an alignment fixture, a twin-zone split furnace and a high-temperature extensometer. The tests were undertaken using flat specimens of 2 mm thickness and 8 mm width, with 40 mm gauge lengths machined such that the tensile stress axes were parallel (0°) to one of the 0/90° fibre directions. These procedures are the same as those adopted to test the SiC_f–SiC,[9] SiC_f–SiBC[10] and $HNSiC_f$–SiC products.[11] The present experimental methods also gave results indistinguishable from those reported when constant-load creep machines[6] were used with the SiC_f–SiC[6] and SiC_f–$A1_2O_3$ composites.[7]

3. Results and discussion

Over the stress ranges investigated at 1300 °C for the $HNSiC_f$–$A1_3O_3$ and $HNSiC_f$–SiBC samples, the general manner in which the creep strain (ε) increases with time (t) is similar to that reported previously for all other CFCMCs now considered.[6–11] Thus, as illustrated by the ε/t trajectories for the $HNSiC_f$–SiBC material in Fig. 1, following the initial loading strain, the creep rate decays continuously, reaching a minimum rate ($\dot{\varepsilon}_m$) just prior to failure. Little or no period of accelerating tertiary creep is then apparent before fracture occurs after a time (t_f) when the total creep strain reaches the limiting creep ductility (ε_f). Hence, to compare the creep and creep fracture properties of CFCMCs produced with Nicalon™ NLM202 or Hi-Nicalon™ fibres reinforcing $A1_2O_3$, SiC or SiBC matrices, the values of $\dot{\varepsilon}_m$, t_f and ε_f were determined from each creep curve.

3.1. Relative strengths of fibres and matrices

Fig. 2 shows the variations of the minimum creep rate with stress at 1300 °C for SiC_f–$A1_2O_3$[7] and the present $HNSiC_f$–Al_2O_3 material, together with results for an alumina–matrix composite reinforced with 25 vol.% SiC whiskers,[15] now termed SiC_w–$A1_2O_3$. Also included in Fig. 2

Table 1
Distinguishing features of fibre-reinforced composites

Material designation	Fibre type	Matrix material	Interface type	Reference
$HNSiC_f$–Al_2O_3	Hi-Nicalon™	Al_2O_3	BN/SiC	
SiC_f–Al_2O_3	Nicalon™ NLM 202	Al_2O_3	BN/SiC	7
$HNSiC_f$–SiBC	Hi-Nicalon™	Enhanced SiC	Carbon	
SiC_f–SiC	Nicalon™ NLM 202	SiC	Carbon	6,9
SiC_f–SIBC	Nicalon™ NLM 202	Enhanced SiC	Carbon	10
$HNSiC_f$–SiC	Hi-Nicalon™	SiC	Carbon	11

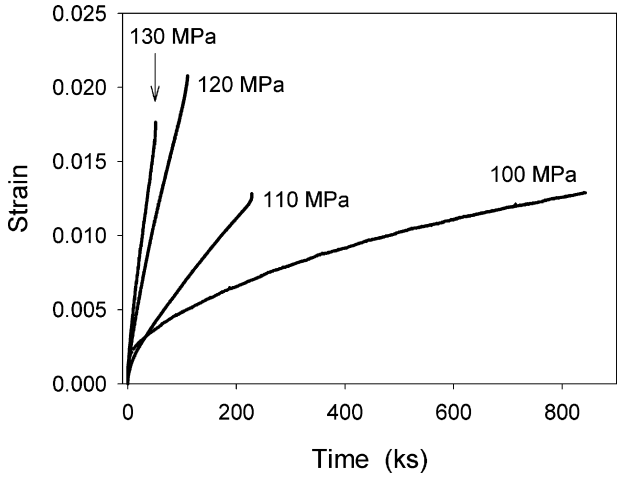

Fig. 1. The variations of the creep strain with time for $HNSiC_f$–SiBC samples tested at various stresses in air at 1300 °C.

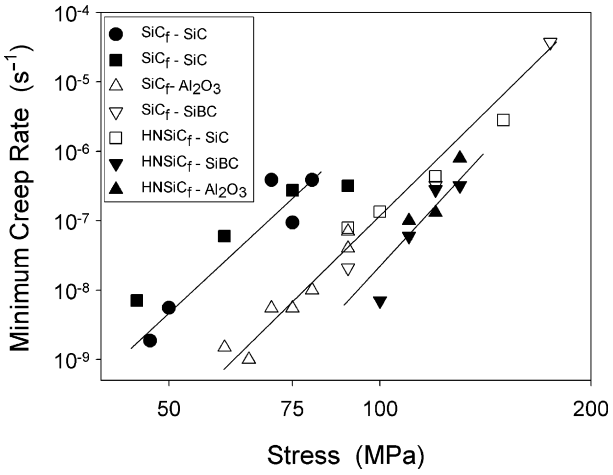

Fig. 3. Comparisons of the stress/minimum creep rate relationships for SiC_f–Al_2O_3[7] and $HNSiC_f$–Al_2O_3, as well as for SiC_f–SiC,[6,9] SiC_f–SiBC,[10] $HNSiC_f$–SiC[11] and $HNSiC_f$–SiBC samples tested in air at 1300 °C.

are $\dot{\varepsilon}_m$ measurements reported for Nicalon™ NLM202 fibres[16] and one $\dot{\varepsilon}_m$ value found for Hi-Nicalon™ fibres.[17]

The presence of 25 vol.% SiC whiskers significantly increases the creep resistance of alumina.[15] The porous $A1_2O_3$ matrices formed by in situ oxidation of liquid aluminium must therefore have creep strengths much lower than that of the fully dense SiC_w–$A1_2O_3$ samples. Yet, at comparable stress levels, the $\dot{\varepsilon}_m$ values for the SiC_w–$A1_2O_3$ specimens are several orders of magnitude faster than those for the $HNSiC_f$–$A1_2O_3$ and SiC_f–$A1_2O_3$ products. Consequently, the alumina matrices make little contribution to the overall creep resistance of the fibre-reinforced composites.[8]

It is also apparent from Fig. 2 that stresses about five times higher must be applied to the Nicalon™ NLM202 and Hi-Nicalon™ fibres to obtain creep rates comparable with those for the SiC_f–$A1_2O_3$ and $HNSiC_f$–$A1_2O_3$ specimens, respectively. This result would be expected because these composites contain 40 vol.% of interwoven 0/90° fibre bundles, so the fibres parallel to the stress axes occupy approximately one fifth of the testpiece cross-sectional areas. Thus, the load-bearing capabilities of the alumina–matrix composites are governed by the longitudinal (0°) fibres.[8]

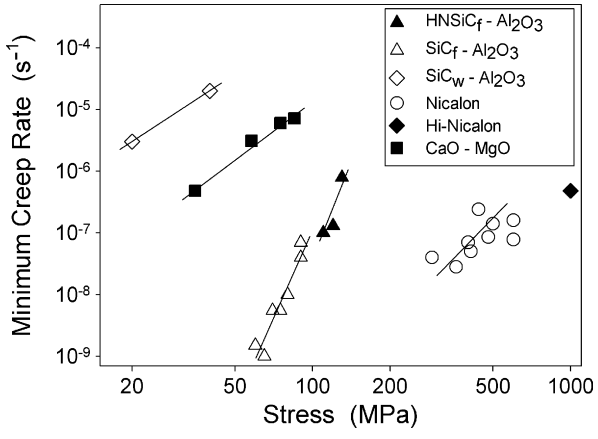

Fig. 2. The stress dependences of the minimum creep rates recorded for the $HNSiC_f$–Al_2O_3 composite in air at 1300 °C compared with data available for SiC_f–Al_2O_3[7] and a SiC whisker-reinforced composite, SiC_w–Al_2O_3.[15] Also included are results reported at 1300 °C for Nicalon™ NLM202[16] and Hi-Nicalon™ fibres.[17] In addition, stress–creep rate values at 1200 °C are shown for synthetic CaO–50% MgO samples (Table 2).

While the creep resistance of the fibres clearly exceeds that of the matrices with the SiC_f–$A1_2O_3$ and $HNSiC_f$–$A1_2O_3$ samples, it has been claimed that the matrices are more creep resistant than the fibres with the SiC_f–SiC,[9] SiC_f–SiBC[10] and $HNSiC_f$–SiC[11] materials. However, as evident from Fig. 3, the $\dot{\varepsilon}_m$ values recorded for the SiC_f–$A1_2O_3$ testpieces are equal to those for the SiC_f–SiBC and lower than those for the SiC_f–SiC specimens, with all three materials being reinforced with comparable volume fractions of 0/90° Nicalon™ NLM202 fibres. Similarly, with equivalent Hi-Nicalon reinforcement, the $\dot{\varepsilon}_m$ values for $HNSiC_f$–$A1_2O_3$ are equal to those for $HNSiC_f$–SiBC and lower than those for the $HNSiC_f$–SiC sample (Fig. 3). Hence, the porous SiC and SiBC matrices must be characterized by a creep resistance at least as poor as that for the weak $A1_2O_3$ matrices.

Irrespective of whether the present series of CFCMCs were produced with $A1_2O_3$, SiC or SiBC matrices, it is therefore clear that the creep strengths of the matrices are markedly inferior to those of the fibres.[8] On this basis, from the results presented in Figs. 3 and 4, the improvement in creep and creep rupture resistance achieved by replacing Nicalon™ NLM202 with Hi-Nicalon™ fibres can be quantified easily.

3.2. Creep data comparisons

CFCMCs obviously display a stochastic strength response because of their essentially brittle character, coupled with the near-random nature of the size and distribution of the macroscopic and microscopic flaws which are present. Even so, recognizing that the $\dot{\varepsilon}_m$ and t_f measurements in Figs. 3 and 4 were obtained for a range of composites tested in two different laboratories,[6–11] the recorded data sets reveal remarkably consistent patterns of property variation as the fibre–matrix combinations are changed.

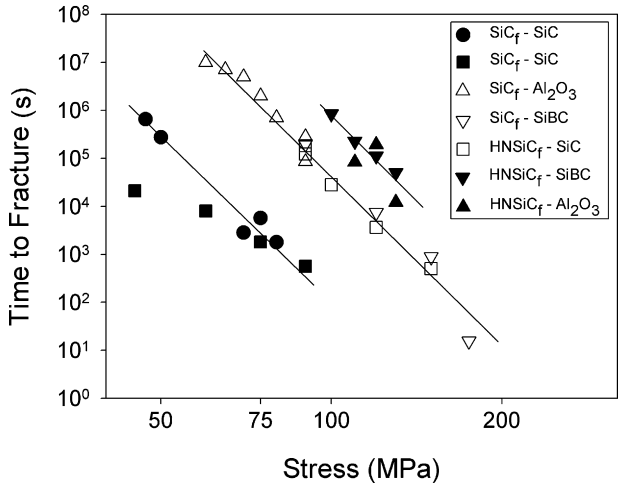

Fig. 4. Comparisons of the stress/creep life relationships for SiC_f–Al_2O_3[7] and $HNSiC_f$–Al_2O_3, as well as for SiC_f–SiC,[6,9] SiC_f–SiBC,[10] $HNSiC_f$–SiC[11] and $HNSiC_f$–SiBC samples tested in air at 1300 °C.

As shown in Fig. 2, with the Al_2O_3–matrix composites, the creep rates at a given stress are reduced by a factor of about 5 by replacing Nicalon™ NLM202 with stronger Hi-Nicalon™ fibres. Similarly, this change in fibre type results in an equivalent enhancement in creep resistance with composites having either SiC or SiBC matrices, as evident from Fig. 3. Moreover, comparisons of the data sets in Figs. 3 and 4 demonstrate that fibre–matrix combinations which improve creep resistance also lead to substantially longer creep lives. This result would be expected because the creep life is often inversely proportional to the minimum creep rate (Fig. 5), such that

$$\dot{\varepsilon}_m t_f \cong \text{constant} \quad (1)$$

showing that the rates at which creep damage develops to cause fracture are determined by the rates of creep strain accumulation, i.e. creep failure is strain controlled. Yet, with the present CFCMC's, the magnitude of $\dot{\varepsilon}_m t_f$ is both material and test condition sensitive.

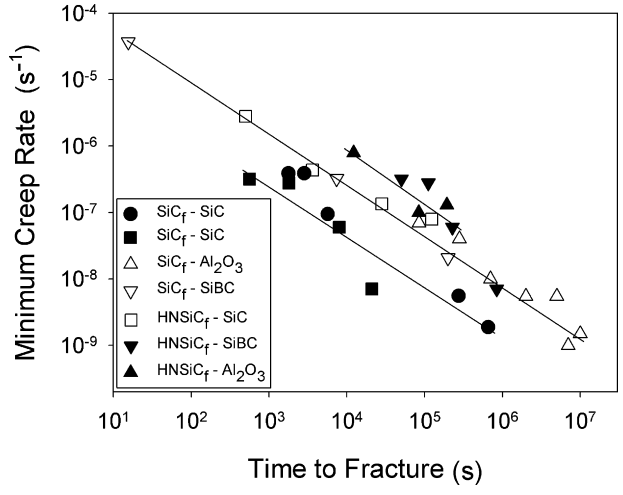

Fig. 5. The dependences of the rupture life on the minimum creep rate for SiC_f–Al_2O_3[7] and $HNSiC_f$–Al_2O_3, as well as for SiC_f–SiC[6,9] and SiC_f–SiBC,[10] $HNSiC_f$–SiC[11] and $HNSiC_f$–SiBC samples tested in air at 1300 °C.

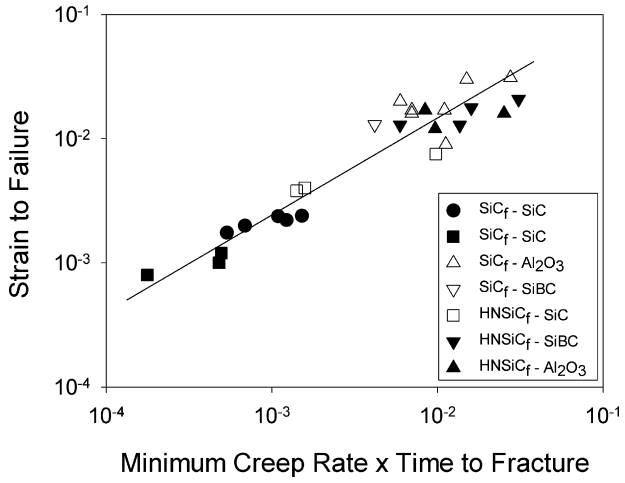

Fig. 6. The relationship between the product, $\dot{\varepsilon}_m t_f$, and the creep ductility (ε_f) for SiC_f–Al_2O_3[7] and $HNSiC_f$–Al_2O_3, as well as for SiC_f–SiC,[6,9] SiC_f–SiBC,[10] $HNSiC_f$–SiC[11] and $HNSiC_f$–SiBC samples tested in air at 1300 °C.

As the applied stress is decreased over the ranges covered at 1300 °C, $\dot{\varepsilon}_m t_f$ increases from ~0.0002 to 0.002 with the SiC_f–SiC samples,[6,9] from ~0.002 to ~0.04 with the SiC_f–Al_2O_3,[7] SiC_f–SiBC[10] and $HNSiC_f$–SiC[11] and from ~0.008 to ~0.04 with the present $HNSiC_f$–Al_2O_3 and $HNSiC_f$–SiBC products (Fig. 5). Moreover, these increases in $\dot{\varepsilon}_m t_f$ are matched by increases in creep ductility (ε_f) as the stress is reduced (Fig. 6), indicating that

$$\dot{\varepsilon}_m t_f = \chi \varepsilon_f \quad (2)$$

with χ increasing from ~0.4 to 0.7 with increasing test duration. This relationship between $\dot{\varepsilon}_m t_f$ and ε_f, as well as the results presented in Figs. 2–6, can then be explained[8] by reference to the ε/t trajectories included in Fig. 7.

3.3. Variations in creep curve shape

Under uniaxial tension, the creep rupture life (t_f) can be defined conveniently as the time taken for the accumulated creep strain (ε) to become equal to the limiting creep ductility, speci-

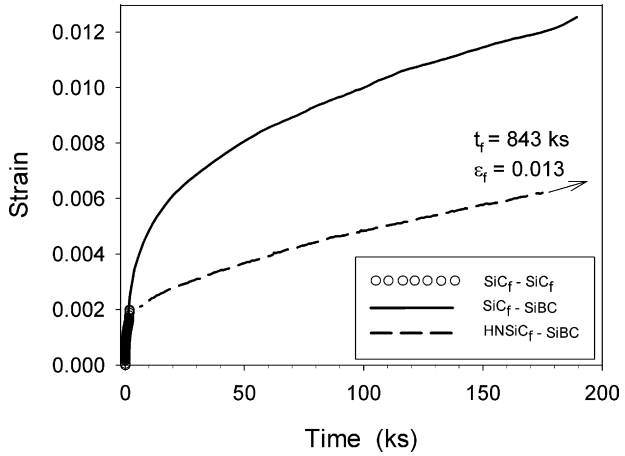

Fig. 7. Creep strain–time curves recorded for SiC_f–SiC,[6] SiC_f–SiBC[10] at 90 MPa and a $HNSiC_f$–SiBC specimen at 100 MPa for tests in air at 1300 °C.

fied as the total creep strain to failure (ε_f). Continuously decaying creep strain/time curves of the form shown in Figs. 1 and 7 therefore terminate when $t = t_f$ and $\dot{\varepsilon} \cong \dot{\varepsilon}_m$ when $\varepsilon = \varepsilon_f$.

In this context, with the SiC_f–SiC composite, the creep ductilities are very low (Fig. 6) so the creep curves terminate early (Fig. 7), giving high $\dot{\varepsilon}_m$ and low t_f values (Figs. 3 and 4). Although the initial rates of creep strain accumulation are similar because the fibre reinforcement is essentially the same, the creep ductilities of the SiC_f–SiBC material are higher than those for the SiC_f–SiC samples (Fig. 6). Creep therefore continues until the larger ε_f values are attained, so lower creep rates and much longer creep lives are displayed under the same test conditions (Fig. 7). Then, by replacing the Nicalon™ NLM 202 with stronger Hi-Nicalon™ fibres, the rates of creep strain accumulation are also decreased (Fig. 7), so the large ε_f values (Fig. 6) lead to the creep and creep rupture strength of the $HNSiC_f$–SiBC composite being considerably superior to the properties displayed by the SiC_f–SiBC specimens (Figs. 3 and 4). Yet, while substantial performance gains would be anticipated by incorporation of stronger fibres, the matrices contribute little to the stress-bearing capabilities of these CFCMCs. Even so, with nominally identical fibre reinforcement, replacing SiC with either SiBC or Al_2O_3 matrices leads to significant strength enhancements (Figs. 3 and 4). This observation can then be interpreted by considering the deformation and damage processes governing strain accumulation and failure.

3.4. Creep deformation and damage processes

On applying a tensile load to a 'textile' CFCMC, the interwoven longitudinal fibre bundles extend and straighten in the stress direction. However, as with the individual fibres,[16] the creep strengths of fibre bundles also vary.[18] Hence, the weakest fibre regions deform most easily, so the high initial creep rates decrease with time as load is transferred progressively to stronger bundles. This deformation is accompanied by crack formation in the brittle matrices but, because the matrices are weak, crack development has little effect on the overall strength of the composite. Consequently, the creep rate continues to decrease with time (Figs. 1 and 7), with the rate of strain accumulation decreasing as the stress and temperature decrease.

As the longitudinal bundles extend and straighten, the resulting complex stress state leads to crack formation within and between the 0° and 90° fibre tows, although composite failure is governed by the growth of 'macro-cracks' along planes normal to the tensile axis.[8] These 'tunnelling' cracks easily by-pass fibres in the 90° bundles (Fig. 8) but, on penetrating into the 0° tows, the cracks become bridged by unbroken longitudinal fibres. Cracks can then open and extend only at rates determined by the creep resistance of the bridging fibres, accounting for the dependence of t_f on $\dot{\varepsilon}_m$ (Fig. 5).

Unfortunately, in oxidizing environments, matrix cracking promotes oxygen ingress, causing premature failure of the crack-bridging fibres and accelerating crack growth.[8] In general, the dominant crack causing failure is surface nucleated (Fig. 9a), developing until the stress on the remaining unbroken cross-section of the composite reaches the critical level at which

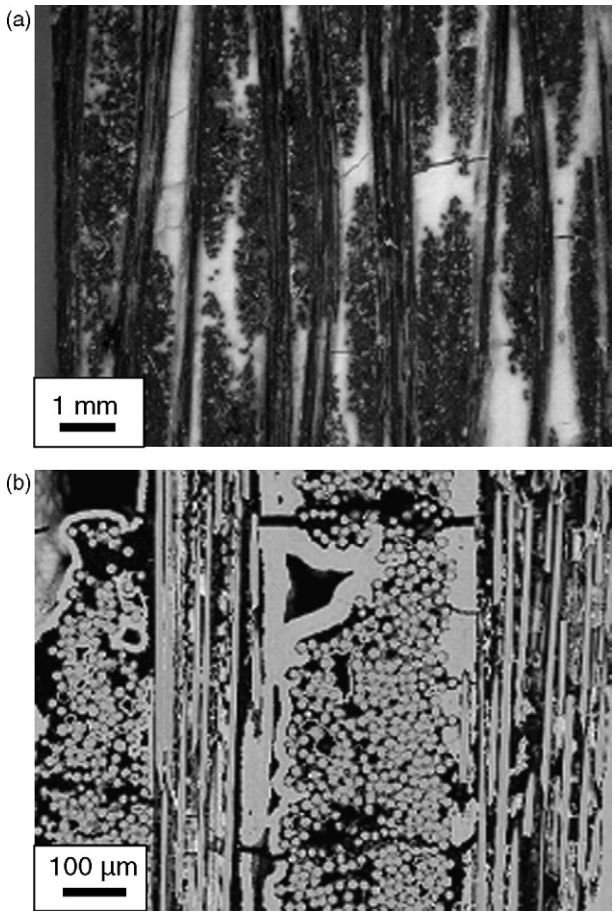

Fig. 8. Scanning electron micrographs showing crack development through the transverse (90°) fibre bundles, by-passing the fibres as the cracks grow through: (a) the alumina matrix of the $HNSiC_f$–Al_2O_3 and (b) the SiBC matrix of the $HNSiC_f$–SiBC composites. In both cases, the tensile stress axis is vertical.

fracture takes place by fibre pull-out (Fig. 9b). In this way, the longitudinal 0° fibres control the rates of strain accumulation and crack growth, while the matrices affect the rates of oxidation-assisted fibre failure and creep ductility.[8]

With the SiC_f–SiC samples,[6] the dominant macro-crack nucleates at surface macro-pores, with direct oxygen penetration along the crack leading to low ductility failure (Fig. 7). In contrast, with the SiC_f–SiBC material, glass formation limits oxidation-assisted fibre failure, giving higher creep ductilities (Fig. 7). Further performance gains are then achieved with the $HNSiC_f$–SiBC product, when the benefits of the enhanced SiBC matrices are combined with the reduced rates of strain accumulation achieved by replacing Nicalon™ NLM202 with Hi-Nicalon™ fibres (Fig. 7).

With alumina matrices, residual stress-induced micro-cracks are present in the as-produced samples,[19] so many small cracks develop throughout the gauge length of the Al_2O_3–matrix composites as creep proceeds.[7] Indirect oxygen ingress through the micro-cracked matrices, coupled with the more oxidation-resistant double BN/SiC interfaces, then results in a resistance to oxidation-assisted fibre failure equivalent to that of SiBC matrices. Hence, similar creep and creep rupture strengths are exhibited by the SiC_f–Al_2O_3 and SiC_f–SiBC materials, as

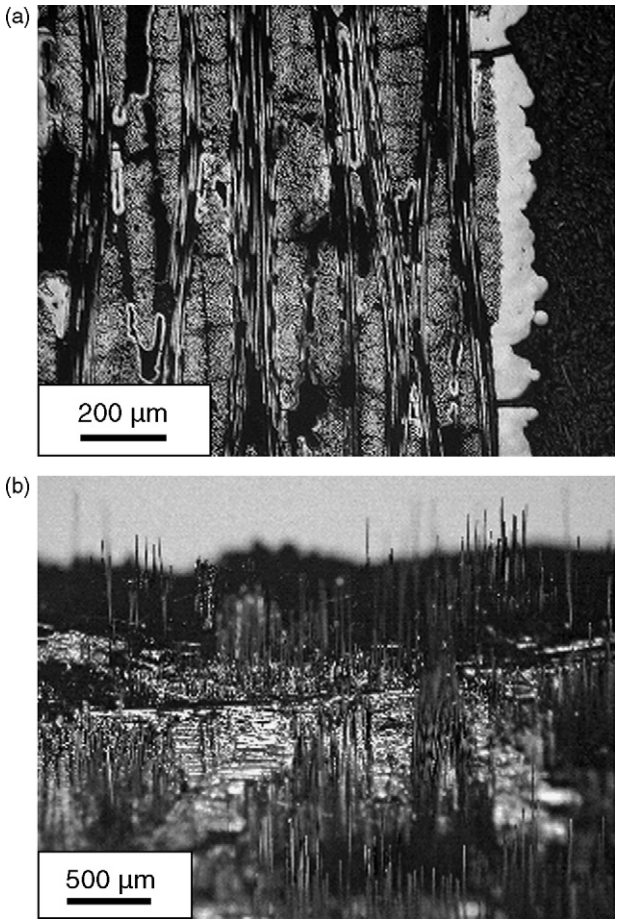

Fig. 9. Scanning electron micrographs showing: (a) nucleation of cracks normal to the tensile axis in the SiBC surface layer and (b) regions of fibre pull-out on the fracture surface of the HNSiC$_f$–SiBC composite tested in air at 1300 °C.

well as by the HNSiC$_f$–Al_2O_3 and HNSiC$_f$–SiBC composites (Figs. 3 and 4).

3.5. Creep in oxidizing environments

As demonstrated in Figs. 3 and 4, product development initiatives such as the introduction of Hi-Nicalon™ fibres and partially self-sealing SiBC matrices have resulted in substantial improvements in the creep and creep fracture strength of SiC fibre-reinforced composites. Even so, for aeroengine and related applications, the resulting component life enhancement may not be as impressive as the increased product costs might imply for several reasons.

(1) With the problem of oxidation-assisted fibre failure caused predominantly by cracking of the weak porous matrices, a low design stress limit must be imposed for components serving in non-protective atmospheres.
(2) Because Nicalon™ NLM202, Hi-Nicalon™ and other types of SiC fibres display continuously decaying creep curves,[16,17] similar curve shapes are exhibited by SiC fibre-reinforced materials (Figs. 1 and 7). In the absence of clearly defined tertiary stages, these woven composites must be recognized as showing creep brittle behaviour, i.e. $\varepsilon_f/\varepsilon_p \cong 1$, where ε_p is the primary creep strain and ε_f is the total creep strain to failure.[20]
(3) Although large cracks can develop before creep failure finally occurs under low applied stresses, so that the present CFCMCs can be regarded as 'crack tolerant', these creep brittle materials have low creep damage tolerance values (λ), where λ can be defined[21] as

$$\lambda = \left[1 + \left(\frac{\varepsilon_t}{\dot{\varepsilon}_m t_f}\right)\right] \quad (3)$$

so $\lambda = 1$ because $\varepsilon_t \cong 0$ (Figs. 1 and 7). The creep damage tolerance value is important in practical situations when materials must withstand local strain concentrations, say, in regions where a change in component cross-section leads to stress concentrations.[22] Values of λ in the range 5–10 are then thought to ensure that the strain concentrations encountered during service will not lead to premature failure.[22] Hence, with the SiC$_f$-reinforced composites now considered, λ values near unity may represent a severe design constraint. For this reason, alternative fibre–matrix combinations should be considered for safety-critical aeroengine and related applications.

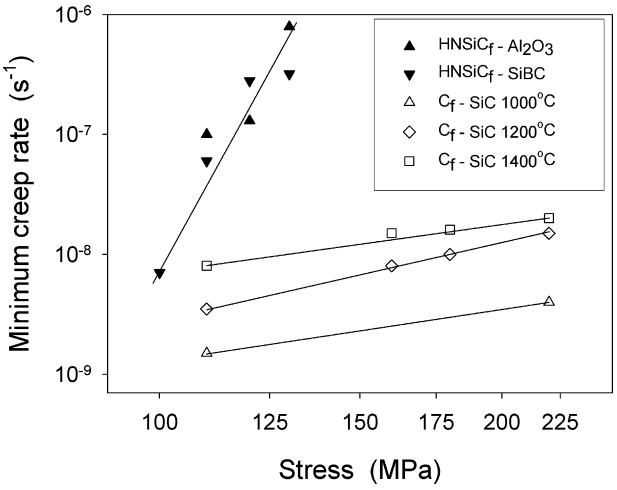

Fig. 10. The stress dependences of the minimum creep rates recorded for the HNSiC$_f$–Al_2O_3 and HNSiC$_f$–SiBC composites in air at 1300 °C, compared with results reported for 2.5D C$_f$–SiC samples[24] tested under low pressure argon at 1200–1400 °C.

Interestingly, even when compared with the results now documented for the high-performance HNSiC$_f$–Al_2O_3 and HNSiC$_f$–SiBC products, the impressive creep resistance of a carbon fibre-reinforced SiC–matrix composite[23,24] is illustrated in Fig. 10. The carbon fibres were again introduced as 2D woven bundles, but with the carbon fabric layers interlinked to avoid delamination, giving 2.5D C$_f$–SiC testpieces. However, the data sets for the 2.5D C$_f$–SiC samples were determined under low-pressure argon. Hence, a major reduction in creep life and ductility will occur when crack development in the brittle SiC matrix allows oxygen penetration during creep in non-protective atmospheres.

Research emphasis has also been directed to oxide fibre-reinforced composites, with the oxide fibres seemingly less liable to oxidation-assisted failure.[3] Yet, as expected for the 2.5D C_f–SiC product, creep data sets reported for an Al_2O_3-fibre-reinforced SiC–matrix composite have emphasized the marked reduction in creep life and ductility caused by testing in air rather than vacuum.[25] Moreover, in seeking to identify suitable oxide–oxide composites, the creep strengths of currently available oxide fibres are inferior to the values for the established SiC fibres.[3]

Clearly, irrespective of the fibre type chosen, the principal creep life-limiting phenomenon encountered with woven CFCMCs operating under load in non-protective atmospheres at high temperatures is premature fibre failure associated with oxygen ingress as cracks develop in the brittle matrices. For this reason, to protect the vulnerable fibres and fibre–matrix interfaces, it is now proposed that major benefits could be realized by considering composites fabricated with creep damage-resistant matrices, i.e. high-melting point ceramic matrices not prone to creep crack formation.

3.6. Creep of CaO·MgO ceramics

Just as cracks develop in the brittle SiC, SiBC and Al_2O_3 matrices of the SiC fibre-reinforced composites, during tensile creep, intergranular cracks form extensively on the transverse grain boundaries of most polycrystalline ceramics produced in monolithic form, as found for both sintered silicon carbide[26] and alumina.[27] Even during creep in compression, intergranular damage accumulates on boundaries experiencing tensile hoop and radial stresses, in line with the stress distributions predicted using finite element methods.[28] Yet, while creep cracks are evident after compressive creep strains of only a few percent with polycrystalline MgO (Fig. 11a), as well as with CaO, crack formation was not observed[29–31] during compressive creep of two-phase CaO–MgO (doloma) specimens containing ~42–50 wt% MgO (Fig. 11b).

The CaO–MgO system is a simple eutectic, with an eutectic composition of CaO–32 wt% MgO and an eutectic temperature of ~2300 °C. With increasing MgO content, the microstructure changes from a lime crystal matrix enclosing equiaxed magnesia grains to a periclase grain network surrounding equiaxed lime crystals. For a series of CaO–MgO samples varying in composition from 0 to 100 wt% MgO,[31] creep cracks were not discernible in specimens containing around 50 wt% MgO, whereas intergranular damage was readily apparent with samples produced with 0, 25, 75 and 100 wt% MgO. Thus, cracks evolve preferentially on CaO–CaO and MgO–MgO boundaries rather than on CaO–MgO interfaces. In this context, it should be noted that doloma testpieces produced with around 40–50 wt% MgO were not prone to creep crack formation, irrespective of whether the samples were fabricated using synthetic CaO and MgO powders or natural dolomite ($CaCO_3$·$MgCO_3$), as listed in Table 2.

The composition dependence of creep crack development in the synthetic CaO–MgO ceramics was confirmed[31] by differences in the shapes of the ε/t trajectories observed at 1327 °C, as illustrated in Fig. 12. Even under compressive creep conditions, with testpieces containing 0, 25, 75 and 100% MgO, the decaying primary stages give way to accelerating tertiary deformation as the crack incidence increases with increasing creep strain. However, in the absence of crack formation or any other damage process which can cause a tertiary acceleration with the microstructurally stable CaO–50% MgO samples, continuously

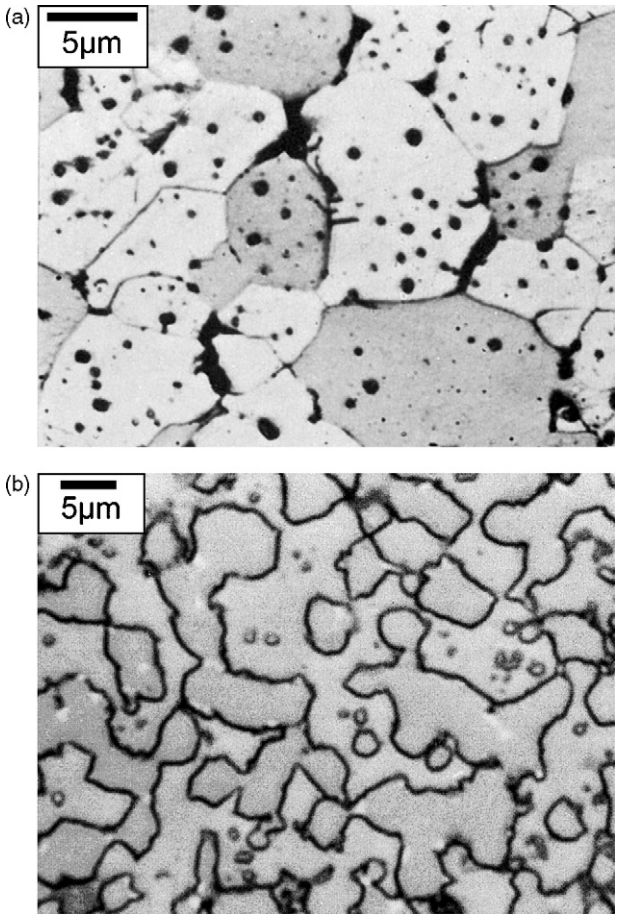

Fig. 11. (a) Intergranular cracking of porous magnesia after a strain of 0.05 at 75 MPa and 1327 °C and (b) the microstructure of natural doloma after a strain of 0.08 at 62 MPa and 1127 °C.[29] The compression axis is vertical.

Table 2
Fabrication procedures, analyses (wt%) and microstructures of natural and synthetic doloma[30]

	Natural doloma	Synthetic doloma
Starting material	Whitwell dolomite ($CaCO_3$·$MgCO_2$)	Analar $Mg(OH)_2CaCO_3$
Calcination temperature (°C)	1300	1300
Sintering temperature (°C)	1600	1800
Porosity of sintered bars (%)	~4–6	~4–6
Average crystal size (μm)	3–5	12–16
Compositions		
CaO	58.02	56.53
MgO	40.53	42.32
SiO_2	0.49	0.76
Al_2O_3	0.03	0.10
Fe_2O_3	0.77	0.13
Other oxides	0.15	0.16

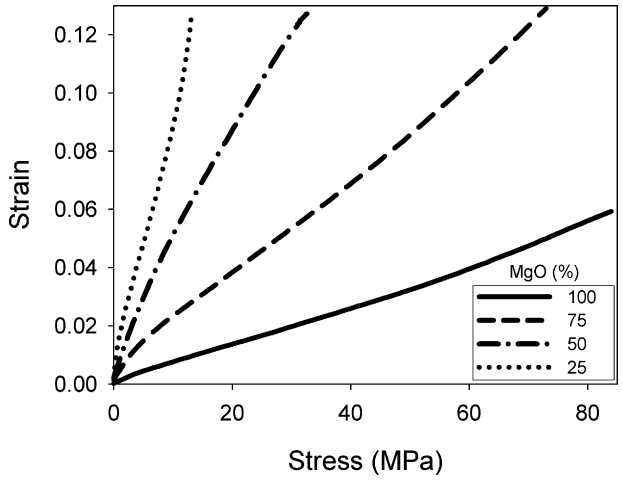

Fig. 12. The effect of variations in MgO content on the creep strain/time curves recorded for synthetic CaO–MgO samples tested under compressive stresses of 62 MPa at 1327 °C.[31]

decaying creep curves were always recorded, i.e. after loading, the creep rate decreases gradually and creep cracking was not discernible[29–31] after true creep strains up to 0.25 (when the tests were discontinued). On this basis, doloma appears to represent a creep damage-resistant option as a matrix for fibre-reinforced composites.

3.7. Potential doloma–matrix composites

Although creep damage resistance is a critical requirement, several additional property features are relevant to consideration of doloma as a candidate matrix material for high-performance CFCMCs.

(a) With synthetic CaO–MgO ceramics, the creep resistance increases with increasing MgO content,[31] with the natural product having a lower creep strength than the synthetic CaO–50% MgO material due to the marginally lower MgO level, higher impurity levels and finer average crystal size (Table 2). At temperatures around 1300 °C, the synthetic CaO–50% MgO samples exhibit creep strengths better than those recorded for the SiC_w–Al_2O_3 ceramic, as evident from Fig. 1. However, the present analysis confirms that the weak SiC, SiBC and Al_2O_3 matrices make little contribution to the overall creep resistance of the present set of SiC fibre-reinforced composites,[8] so the creep strength of the CaO–45 wt% MgO samples is non-critical.
(b) Calcined natural doloma products can deteriorate by 'perishing' during storage, which occurs as a result of moisture attacking the lime phase. Yet, with fully sintered samples of both natural and synthetic doloma (Table 2), no evidence of surface attack was apparent even after several years of atmospheric exposure at room temperature.
(c) Unfortunately, doloma is likely to react with both silicon carbide and oxide fibres at high temperatures, indicating that CaO–MgO matrices would be better employed with less-expensive carbon fibre reinforcement. Certainly, the compatibility of CaO–MgO ceramics with carbon in aggressive oxidizing environments at 1600 °C and above is evident from the dominant selection of carbon-bearing doloma linings for the original Thomas or basic Bessemer process and graphite-bearing magnesia linings for modern basic oxygen steel-making vessels.

The potential success of C_f–doloma composites would depend critically on fabrication methods being devised to obtain low-porosity matrices, free from the inter-connected pores which would provide channels for oxygen ingress. If low-porosity creep damage-resistant CaO–45 wt% MgO matrices can be developed, the impressive creep properties of the C_f–SiC material in argon (Fig. 10) may be attainable with C_f–doloma composites in oxidizing atmospheres.

4. Conclusions

The improvements in creep and creep rupture strength achieved through different fibre–matrix combinations are assessed for composites produced with SiC or SiBC matrices (with carbon interfaces) or Al_2O_3 matrices (with double BN/SiC interfaces), reinforced with either Nicalon™ NLM202 or Hi-Nicalon™ fibres. This comparison of tensile data sets recorded in air at 1300 °C demonstrates the substantial performance gains derived when Hi-Nicalon™ fibres are used with either SiBC or Al_2O_3 matrices.

For the product range considered, the fibres aligned parallel to the tensile stress axes govern the rates of creep strain accumulation and crack growth. However, in non-protective atmospheres, the principal creep life-limiting phenomenon is premature fibre failure associated with oxygen penetration as cracks develop in the brittle matrices. Yet, while crack formation occurs during creep of the SiC, SiBC and Al_2O_3 matrix materials, as well as with most monolithic ceramics, such damage is not discernible with two-phase CaO–45 wt% MgO (doloma). Provided that process routes can be devised to obtain fine-grain low-porosity doloma matrices, free from interconnected pores allowing oxygen ingress, C_f–doloma composites could represent a relatively inexpensive creep damage-resistant option for high temperature applications involving long-term service under load in oxidizing environments.

References

1. Ruffles, P., *Aerospace Structural Materials: Present and Future*. The Institute of Materials, London, 1995.
2. Miller, S., Advanced materials means advanced engines. *Interdiscipl. Sci. Rev.*, 1996, **21**, 2.
3. Parlier, M. and Ritti, M. H., State of the art and perspectives for oxide–oxide composites. *Aerospace Sci. Tech.*, 2003, **14**, 1.
4. Heredia, F. E., McNulty, J. C., Zok, F. W. and Evans, A. G., Oxidation embrittlement probe for ceramic–matrix composites. *J. Am. Ceram. Soc.*, 1995, **78**, 2097.
5. Jones, R. H., Henager Jr., C. H. and Windish Jr., C. F., High temperature corrosion and crack growth of SiC–SiC at variable oxygen partial pressures. *Mater. Sci. Eng. A*, 1995, **A198**, 103.
6. Wilshire, B., Carreño, F. and Percival, M. G. L., Tensile creep and creep fracture of a fibre-reinforced SiC–SiC composite. *Scr. Mater.*, 1998, **39**, 729.

7. Wilshire, B. and Carreño, F., Deformation and damage processes during tensile creep of ceramic-fibre-reinforced ceramic–matrix composites. *J. Eur. Ceram. Soc.*, 2000, **20**, 463.
8. Wilshire, B., Creep property comparisons for ceramic-fibre-reinforced ceramic–matrix composites. *J. Eur. Ceram. Soc.*, 2002, **22**, 1329.
9. Zhu, S., Mizuno, M., Kagawa, Y., Cao, J., Nagano, Y. and Kaya, H., Creep and fatigue behaviour of SiC fibre reinforced SiC composite at high temperatures. *Mater. Sci. Eng. A*, 1997, **225**, 69.
10. Zhu, S., Mizuno, M., Nagano, Y., Cao, J., Kagawa, Y. and Kaya, H., Creep and fatigue behaviour of an enhanced SiC–SiC composite at high temperatures. *J. Am. Ceram. Soc.*, 1998, **81**, 2269.
11. Zhu, S., Mizuno, M., Kagawa, Y., Cao, J., Nagano, Y. and Kaya, H., Creep and fatigue behaviour in Hi-Nicalon^{TM}-fibre-reinforced silicon carbide composites at high temperatures. *J. Am. Ceram. Soc.*, 1999, **82**, 117.
12. Bodet, R., Bourrat, X., Lamon, J. and Naslain, R., Tensile creep behaviour of a silicon-carbide-based fibre with a low oxygen content. *J. Mater. Sci.*, 1995, **30**, 661.
13. Challon, G., Pailler, R., Naslain, R. and Olry, P., Structure composition and mechanical behaviour at high temperature of the oxygen-free Hi-Nicalon^{TM} fibre. In *High-temperature Ceramic–Matrix Composites. II: Manufacturing and Materials Development*, ed. A. G. Evans and R. Naslain. Am. Ceram. Soc., Westerville, OH, 1995, p. 299.
14. Fox, D. S. and Nguyan, Q. N., Oxidation kinetics of enhanced SiC–SiC. *Ceram. Eng. Sci. Proc.*, 1995, **16**, 877.
15. O'Meara, C., Suihkonen, T., Hansson, T. and Warren, R., A microstructural investigation of the mechanisms of tensile creep deformation in an Al_2O_3–SiC_w composite. *Mater. Sci. Eng. A*, 1996, **209**, 251.
16. Simon, G. and Bunsell, A. R., Creep behaviour and structural characterization at high temperature of Nicalon^{TM} SiC fibres. *J. Mater. Sci.*, 1984, **19**, 3658.
17. Challon, G., Pailler, R., Naslain, R. and Olry, P., Correlation between microstructure and mechanical behaviour at high temperatures of a SiC fibre with a low oxygen content (Hi-Nicalon). *J. Mater. Sci.*, 1997, **32**, 1133.
18. Yun, H. M. and DiCarlo, J. A., Thermo-mechanical behaviour of advanced SiC fibre multi-filament tows. *Ceram. Eng. Sci. Proc.*, 1996, **17A**, 61.
19. Heredia, F. E., Evans, A. G. and Andersson, C. A., Tensile and shear properties of continuous fibre-reinforced SiC/Al2O3 processed by melt oxidation. *J. Am. Ceram. Soc.*, 1995, **78**, 2790.
20. Goodall, I. N., Cockcroft, R. D. H. and Chubb, E. J., An approximate description of the creep rupture of structures. *Int. J. Mech. Sci.*, 1975, **17**, 351.
21. Wilshire, B. and Burt, H., Tertiary creep of metals and alloys. *Z. Metallkd.*, 2005, **96**, 552.
22. Leckie, F. A. and Hayhurst, D. R., Constitutive equations for creep rupture. *Acta Metall.*, 1977, **25**, 1059.
23. Botier, G., Vicens, J. and Chermant, J. L., Understanding the creep behaviour of a 2.5D C_f–SiC composite I. Morphology and microstructure of the as-received material. *Mater. Sci. Eng. A*, 2000, **279**, 73.
24. Botier, G., Chermant, J. L. and Vicens, J., Understanding the creep behaviour of a 2.5D C_f–SiC composite II. Experimental specification and macroscopic mechanical creep responses. *Mater. Sci. Eng. A*, 2000, **289**, 265.
25. Lamouroux, F., Steen, M. and Vallés, J. L., Damage of a 2D Al_2O_3–SiC composite during uniaxial creep. *Comp. Sci. Technol.*, 1996, **56**, 825.
26. Wilshire, B. and Jiang, H., Deformation and failure processes during tensile creep of sintered silicon carbide. *Brit. Ceram. Trans.*, 1994, **93**, 213.
27. Folweiler, R. C., Creep behaviour of pore-free polycrystalline aluminium oxide. *J. Appl. Phys.*, 1961, **32**, 773.
28. Birch, J. M., Wilshire, B., Owen, D. R. J. and Shantaram, D., The influence of stress distribution on the deformation and fracture behaviour of ceramic materials under compressive creep conditions. *J. Mater. Sci.*, 1976, **11**, 1817.
29. Wilshire, B., Microstructure dependence of the creep and creep fracture behaviour of ceramic materials. *J. Microsc.*, 1981, **124**, 249.
30. Coath, J. A. and Wilshire, B., Deformation processes during high-temperature creep of lime, magnesia and doloma. *Ceram. Int.*, 1977, **3**, 103.
31. Coath, J. A. and Wilshire, B., The influence of variations in composition on the creep behaviour of doloma. *Ceram. Int.*, 1978, **4**, 66.